Int. J. Electrochem. Sci., 17 **(2022)** Article Number: 221264, doi: 10.20964/2022.12.66

International Journal of
ELECTROCHEMICAL
SCIENCE
www.electrochemsci.org

Synthesis of Graphitic Carbon Nitride and Polypyrrole Nanocomposite (PPy/g-C_3N_4) as Efficient Photocatalysts for Dibenzothiophene Degradation in Oilfield Produced Wastewater

Qiang Liu[1], *Zhigang Zhai*[2], *Jianyi Sun*[3], *Yuyu He*[3], *Zebo Yuan*[3], *Shijun Chen*[4,*]

[1] Traim Oilfield Company, PetroChina, Korla, 841000, Xinjiang, China
[2] Department of Quality, Safety and Environmental Protection, Traim Oilfield Company, PetroChina, Korla, 841000, Xinjiang, China
[3] Experimental and Testing Research Institute， Traim Oilfield Company, PetroChina, Korla, 841000, Xinjiang, China
[4] College of Chemistry and Chemical Engineering, Xi'an SHIYOU University, Xi'an, 710065, Shaanxi Province, P.R.China
[*]E-mail: csj19792018@sina.com

Received: 4 October 2022 / *Accepted:* 2 November 2022 / *Published:* 27 December 2022

This study focused on the chemical preparation of g-C_3N_4 and nancomposite of polypyrrole (PPy) g-C_3N_4 (PPy/g-C_3N_4) and characterization of structural, electrochemical and optical properties, as well as photocatalytic applicability for the removal of dibenzothiophene (DBT), an emerging organosulfur pollutant from oil field wastewater under exposure to sunlight. Analyses of photocatalyst structure and morphology revealed that the structures of PPy/g-C_3N_4 photocatalysts contained amorphous PPy nanoparticles that were decorated on the massive 2D sheet-like structure with numerous breakages and pores on the g-C_3N_4 sheet surface. Optical analyses revealed that the optical band gap values of g-C_3N_4 and PPy/g-C_3N_4 photocatalysts were determined to be ~2.64 and ~2.29 eV, respectively. This indicated a decrease in the optical band gap of PPy/g-C_3N_4 toward g-C_3N_4, which enhanced the photocatalytic activity of PPy/g-C_3N_4 in the visible light region. Because of the smaller particle size of PPy decorated on the g-C_3N_4 sheet-like structure, electrochemical studies revealed that the synergistic effect between PPy and g-C_3N_4 can effectively improve electrochemical properties and increase electron transfer rate. Photocatalytic removal studies revealed that total DBT treatment was obtained for g-C_3N_4 and PPy/g-C_3N_4 nanocomposite after 125 and 90 minutes of sunlight exposure, respectively. These findings reflect the fast photocatalytic treatment rate of DBT in the presence of PPy/g-C_3N_4 nanocomposite toward g-C_3N_4 and other reported photocatalysts in the literature. The practical photocatalytic degradation capability of PPy/g-C_3N_4 nanocomposite was examined for the treatment of real oilfield wastewater and the results showed the effectual photocatalytic performance of PPy/g-C_3N_4 nanocomposite for the treatment of DBT in genuine oilfield wastewater.

Keywords: Photocatalyst; Polypyrrole; g-C_3N_4; Dibenzothiophene; Organosulfur Pollutant; Oilfield Wastewater

1. INTRODUCTION

Pollutants can leak out of storage tanks during oil and gas production and distribution in the oil industry [1]. Depending on the oil's composition, different types of oil emit varying amounts of a pollutant [2, 3]. Furthermore, when oil is burned for electricity, some toxic compounds are produced that have the potential to cause cancer [4]. Other negative environmental effects of the oil industry include increased greenhouse gas emissions, acid rain, groundwater contamination, and poorer water quality, among others [5, 6]. The oil and gas industries can also affect the destruction of ecosystems and biodiversity loss [7]. When oil pollution spreads over the surface in a thin layer, it stops the oxygen reaching the plants and animals in the water and prevents photosynthesis in plants [8, 9]. Contaminated food supplies can also cause animals to become malnourished or poisoned over time [10].

Dibenzothiophene (DBT, $C_{12}H_8S$) is a sulfur-containing heterocyclic molecule found in petroleum [11-13]. This is an organosulfur compound composed of two benzene rings joined to a central thiophene ring [14-16]. This tricyclic heterocycle, particularly its alkyl substituted derivatives, is abundant in petroleum's heavier fractions [17, 18]. It functions as a keratolytic agent. Studies have found strong evidence based on the DBT and its derivatives may act as cancer inducers, emphasizing their toxicological and environmental significance [19-21].

These substantial environmental and biological issues indicate that removing DBT from oil field wastewater is a substantial challenge. Adsorption [22], chemical oxidation [23], ozonation [24], biodegradation [25], liquid membrane [26], and photocatalysis [27-33] are the conventional procedures for removing the DBT molecules from aqueous media. Many of these treatment techniques are expensive, time-consuming, and ineffectual because they are associated with the formation of chemical bonds that break or breakdown which can result in the formation of significant secondary contamination. Photocatalysis is a low-cost treatment technology for removing oil field contaminants using photocatalysts. As a result, the focus of this study was on the chemical preparation of g-C_3N_4 and PPy/g-C_3N_4 nancomposite, and characterization of structural, electrochemical, and optical properties, as well as photocatalytic applicity for the removal of DBT, an emerging organosulfur pollutant from oil field wastewater under exposure to sunlight.

2. EXPERIMENT

2.1. Preparation of PPy/g-C_3N_4 nancomposite

In order to prepare g-C_3N_4 [34], 10 mM of melamine powder (99%, Sigma-Aldrich) was ultrasonically dissolved into 100 mL of ethylene glycol (99.8%, Merck, Germany). Next, 100 mL of 0.2 M HNO_3 (69%, Sigma-Aldrich) solution was gradually added dropwise into the obtained solution

under magnetic stirring at room temperature. The resultant product was collected and washed by ethanol (99%, Duter Co., Ltd., China) several times. After drying at 55 °C for 4 hours, the obtained powder as a precursor of protonated melamine was put in an alumina boat under heating at 500°C for 120 minutes to achieve the g-C_3N_4. 5 g of the obtained g-C_3N_4 powder and 0.5 g sodium dodecyl benzenesulfonate (SDBS, 80%, Sigma-Aldrich) were ultrasonically dispersed in 120 mL of deionized water for the preparation of the PPy/g-C_3N_4 nanocomposite [35]. Subsequently, 1 wt% of pyrrole (98%, Sigma-Aldrich) was added to the resultant suspension under vigorous stirring in an ice–water bath for 30 minutes. Afterwards, 15 mL of 0.5 M aqueous ferric chloride (97%; Sigma-Aldrich) solution was added dropwise into the mixture. After 120 minutes, the obtained light gray precipitates as nancomposite were filtered under vacuum and washed by a mixture of ethanol and deionized water three times. Then, the PPy/g-C_3N_4 nancomposite was dried at 55°C in an oven for 10 hours.

2.2. Characterizations

The morphological and crystallographic properties of the nanostructures were evaluated using scanning electron microscopy (SEM) on a Hitachi S4300-F microscope (Tokyo, Japan) and an X-ray diffractometer (XRD, Rigaku Miniflex 600, Rigaku, Tokyo, Japan). For cyclic voltammetry (CV) measurements, an electrochemical workstation system (TOB-CS-150, Xiamen Tob New Energy Technology Co., Ltd., China) equipped with a three-electrode electrochemical cell containing Ag/AgCl (reference electrode), platinum mesh (counter electrode), and photocatalysts modified ITO was used. All CV measurements were carried out in an electrolyte containing 1 mM $Fe(CN)_6^{3-/4-}$ (99%).

Photocatalytic experiments were conducted on a pyrex reactor equipped with a circulating water jacket at room temperature to analyze the prepared photocatalysts. As the simulated sunlight source, a 70 W xenon lamp (Changzhou Anshuo Electric Light Source Co., Ltd., China) was placed above the reactor. 0.5 g of prepared photocatalysts were mixed into 200 mL of DBT solutions for photocatalytic reaction with constant stirring. To obtain the desorbance-absorbance balance, prior to light illumination, the resulted suspension was magnetically stirred in the dark atmosphere for about 45 minutes. The stable mixture was then continuously stirred while being exposed to a light source. At regular intervals, the photodegraded DBT sample was collected and centrifuged for 10 minutes at 1000 rpm to remove photocatalyst particles. Finally, a Shimadzu UV-2450 UV-Vis spectrophotometer (Tokyo, Japan) was used for determination of the absorption spectrum of photodegraded DBT and the absorption at λ=254 nm was used to determine the removal efficiency by using the following equation [36-39].

$$\text{Removal efficiency (\%)} = \frac{C_0 - C_t}{C_0} \times 100 \qquad (1)$$

In this equation, C_0 and C_t are reflected as the initial concentration of the DBT and the concentration of the DBT after exposure to sunlight illumination, respectively.

3. RESULTS AND DISCUSSION

3.1. Analyses of structure and morphology of photocatalysts

Figure 1 displays SEM images of g-C_3N_4 and PPy/g-C_3N_4 photocatalysts. Figure 1a shows a variety of loosely aggregated sheet-like g-C_3N_4 structures with irregular shapes. As seen, g-C_3N_4 structures have dense and thick layers that combine to form a massive 2D sheet-like structure, and there are numerous breakages and pores on the surface of the g-C_3N_4 sheets caused by melamine decomposition [40-42]. Figure 1b shows a SEM image of PPy/g-C_3N_4 photocatalysts with small amorphous PPy nanoparticles decorated on dense and thick layers of g-C_3N_4 sheets, confirming the formation of nanocomposite structures.

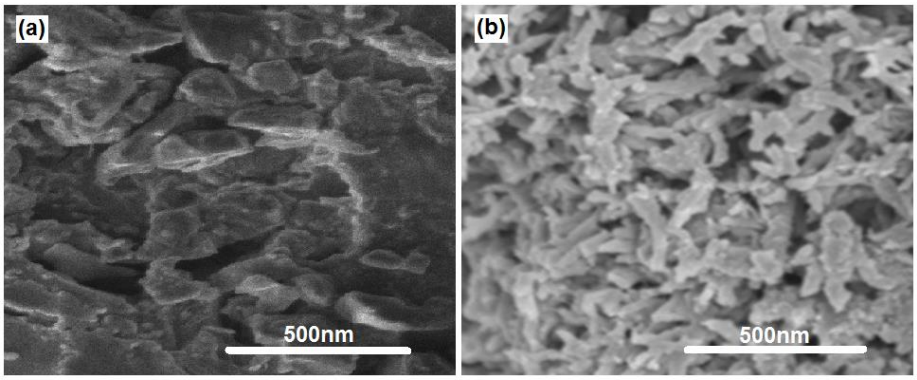

Figure 1. SEM pictures of (a) g-C_3N_4 and (b) PPy/g-C_3N_4.

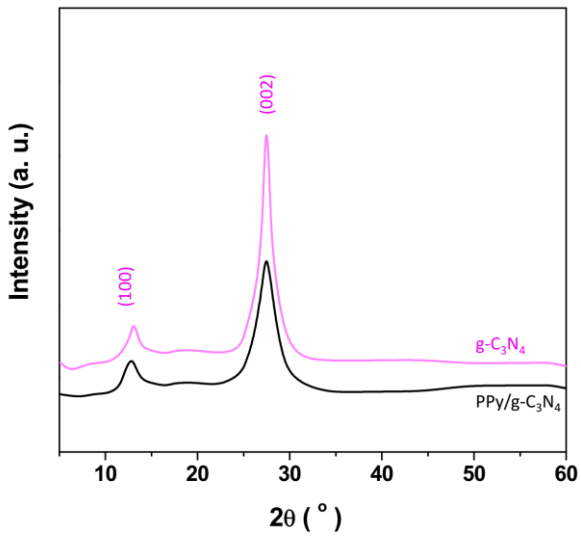

Figure 2. XRD patterns of PPy/g-C_3N_4 and g-C_3N_4.

The XRD patterns of PPy/g-C_3N_4 and g-C_3N_4 are presented in Figure 2. XRD patterns of g-C3N4 and PPy/g-C3N4 show characteristic peaks at 2θ = 12.97° and 27.42°, which are assigned to the (100) and (002) planes, respectively [43, 44]. The lattice plane of (002) is important for the interlayer

stacking of the g-C_3N_4 periodic graphitic conjugated aromatic system [45-47]. The periodic tri-s-triazine ring structure associated with protonated melamine is indexed to the diffraction (100) lattice plane [48-50]. The peak intensity in the XRD pattern of PPy/g-C_3N_4 is decreased toward g-C_3N_4, indicating that PPy influences crystal growth and crystallinity because polymer with amorphous particles is decorated on the sheet-like structures of g-C_3N_4 [51].

3.2. Characterization of photocatalysts optical properties

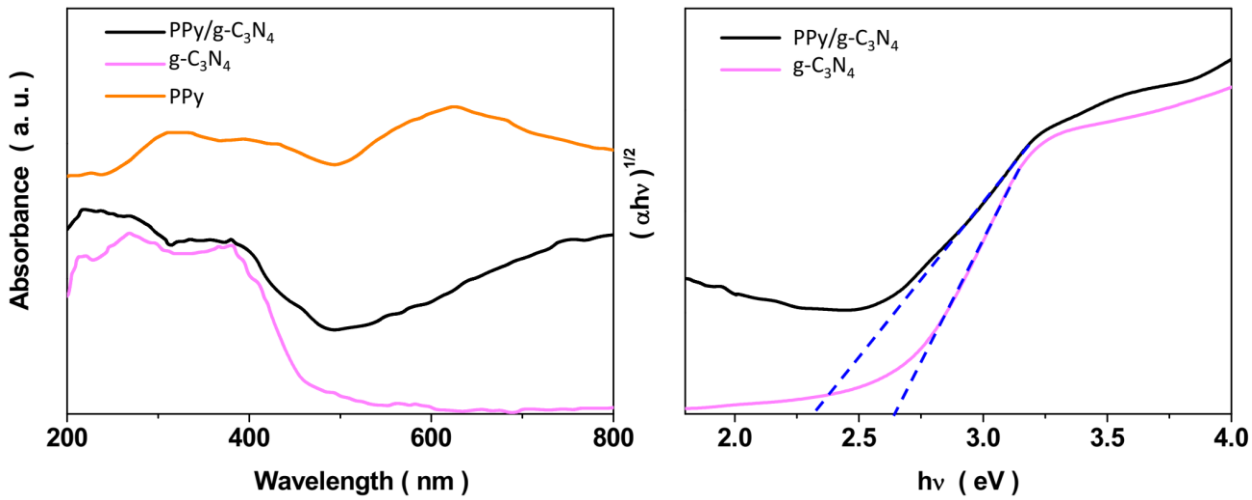

Figure 3. (a) UV–vis absorption spectra of the PPy, g-C_3N_4 and PPy/g-C_3N_4 photocatalysts and (b) Tauc's plots.

Figure 3a depicts the UV-vis absorption spectra of PPy, g-C_3N_4, and PPy/g-C_3N_4. As ssen, the g-C_3N_4 and PPy/g-C_3N_4 nanostructures absorb light in both of the UV and visible regions. Because of the π→π* inter band transition of the PPy molecules, no absorption edge is observed for pure PPy, and UV-vis absorption spectra show great absorption in all wavelengths [52-54]. Pure g-C_3N_4 has a 390 nm absorption edge and shows the absorption over the whole UV and visible light regions [35, 55, 56]. The PPy/g-C_3N_4 exhibits a clear redshift in absorption spectra to 410 nm, which can be related to the enhancement of visible light absorption ability of the nanocomposites with the interaction between PPy and g-C_3N_4 semiconductors in the heterojunctions [57, 58]. As a 2D nanocomposite of PPy and g-C_3N_4 semiconductors, PPy has a more negative conduct band and valance band potential than g-C_3N_4 [59], allowing the formation of type II heterojunctions with efficient density of photo-generated carriers and accelerated hole-electron separation [57, 60]. In a type-II heterojunction, the photo-generated holes transfer to a less positive valence band while the photo-generated electrons to a less negative conduction band, indicating an efficacious charge separation which is more suitable for the photocatalytic reactions [61-63]. The optical band gap energy (Eg) value for photocatalysts can be determined by the following equation [64-66]:

$$(\alpha h\nu)^{1/2} = B(h\nu - Eg) \qquad (2)$$

The absorption coefficient and photon energy are represented by and hv, respectively, in this equation, and B donates to the proportionality parameter. For determination of the Eg values of PPy, g-C_3N_4, and PPy/g-C_3N_4 photocatalysts Tauc's plots can be used to show that it is plotting $(\alpha hv)^{1/2}$ against photon energy (hv) which gives a straight line with an intercept equal to the optical energy band gap, as shown in Figure 3b. The Eg values of g-C_3N_4 and PPy/g-C_3N_4 photocatalysts can be estimated to be ~2.64 and 2.29 eV, respectively. As found, the optical band gap of PPy/g-C_3N_4 decreases toward g-C_3N_4, demonstrating that it can increase photocatalytic activity in visible light regions.

3.3. Electrochemical studies

The electrochemical properties of g-C_3N_4 and PPy/g-C_3N_4 nanocomposite modified ITO electrodes were studied using CV in 1 mM $Fe(CN)_6^{3-/4-}$ electrolyte at a potential range from -0.2 V to 0.6V at a scan rate of 100 mV/s. Figure 4 demonstrates the CV curves of modified electrodes with a pair of redox peaks and a peak-to-peak separation (ΔEp) of 0.17 and 0.08 V for g-C_3N_4 and PPy/g-C_3N_4 nanocomposite modified ITO electrodes, respectively. As seen, the highest peak currents and lowest peak-to-peak separation potential are observed for the PPy/g-C_3N_4 nanocomposite modified ITO electrode, implying the synergistic effect of PPy and g-C_3N_4 can effectively improve the electrochemical properties and enhance the electron transfer rate due to the smaller particle size of PPy decorated on the g-C_3N_4 sheet-like structure which forms a large electroactive surface area and numerous of electro-active sites of the PPy/g-C_3N_4 nanocomposite modified electrode. It is in agreement with the SEM results [67-69].

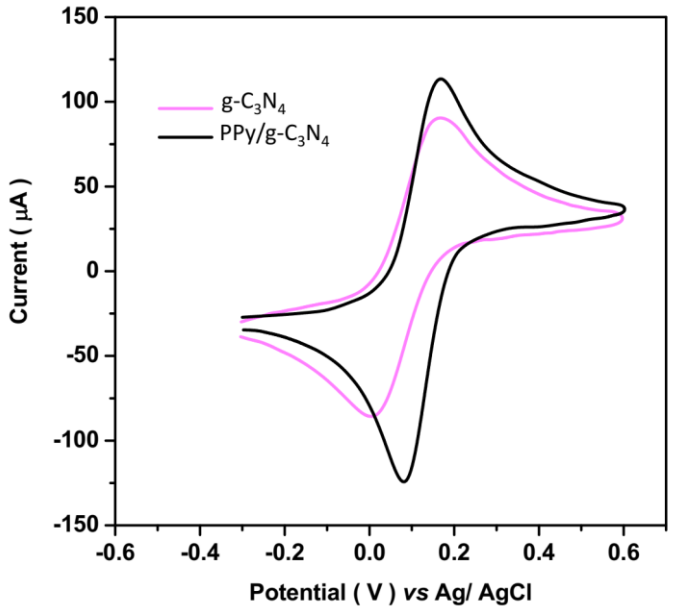

Figure 4. CV curves of g-C_3N_4 and PPy/g-C_3N_4 nanocomposite modified ITO electrode in 1 mM $Fe(CN)_6^{3-/4-}$ electrolyte at potential range -0.2 V to 0.6V at scan rate of 100 mV/s.

3.4. Photocatalytic degradation studies

Figure 5 depicts the removal efficiency of 200 mL of 100 mg/L DBT solution in the absence (blank sample) and presence of photocatalysts. After 150 minutes of exposure to sunlight, the removal efficiency of a blank sample reaches 2.4%. The removal efficiency in the presence of g-C3N4 and PPy/g-C_3N_4 nanocomposite is 43.5% and 50% after 30 minutes of sunlight illumination, respectively, and total DBT treatment is obtained for g-C_3N_4 and PPy/g-C_3N_4 nanocomposite after 125 and 90 minutes of sunlight exposure, respectively.

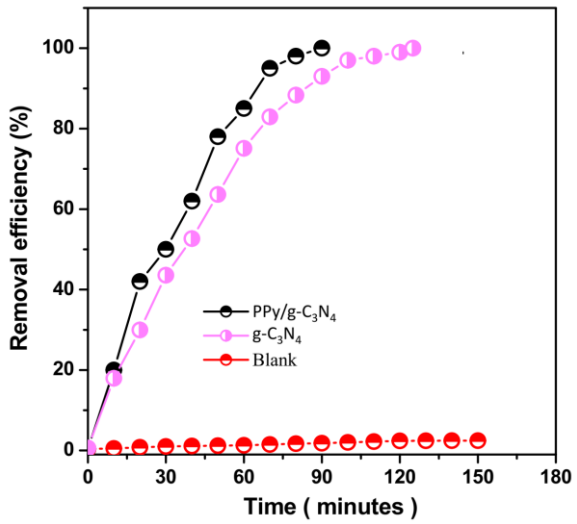

Figure 5. The removal efficiency of 200 ml of 100 mg/L DBT solution in blank sample and presence of g-C_3N_4 and PPy/g-C_3N_4 nanocomposite photocatalysts upon exposure sunlight illumination.

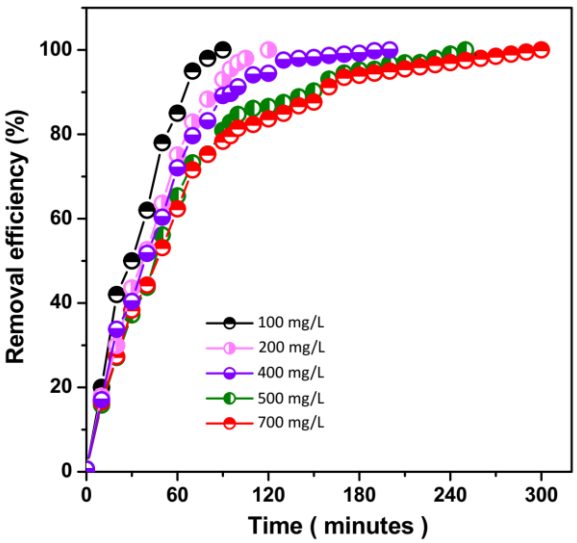

Figure 6. The removal efficiency of PPy/g-C_3N_4 nanocomposite for treatment different concentrations of DBT upon exposure sunlight illumination.

.

Thus, these results reflect a fast photocatalytic treatment rate of DBT in the presence of PPy/g-C3N4 nanocomposite toward the g-C_3N_4, which verifies the results of structural, optical, and electrochemical analyses based on a large effective surface area, the formation of more electro-active sites, and efficient photo-induced electron and hole separation in the created heterojunction between PPy and g-C_3N_4 in PPy/g-C_3N_4 nanocomposite, which can effectually increase the photo-generated carriers spreading distance and prolong the carrier lifetime [70, 71]. During light illumination, the photo-generated electrons can react with O_2 to create the superoxide radical (O_2^-) [72], while the photo-induced holes can react with H_2O and OH^- to generate the hydroxyl radicals ($^{\bullet}OH$) [73, 74]. Thus, the generated O_2 and $^{\bullet}OH$ can act as oxidants for the degradation the DBT on the photocatalyst surface [75].

Figure 6 depicts the removal efficiency of PPy/g-C_3N_4 nanocomposite for treatment of various concentrations of DBT under sunlight illumination. After 90, 120, 200, 250, and 300 minutes of exposure to sunlight, 100, 200, 400, 500, and 700 mg/L of DBT are completely treated. The results show that as the initial DBT concentration increases, the removal efficiency decreases. Furthermore, in Table 2, the photocatalytic activity of the PPy/g-C_3N_4 nanocomposite for DBT treatment is compared to that of previously reported photocatalysts. It is attributed to the synergistic effect between the PPy and g-C_3N_4 in the nanocomposite to create a large efficacious surface area and heterojunction to promote the efficiency in photo-excited electrons and holes population and photocatalytic reactions. It was discovered that the PPy/g-C_3N_4 nanocomposite reflects a fast rate of photocatalytic treatment.

Table 2. The photocatalytic activity of PPy/g-C_3N_4 nanocomposite for treatment DBT and other reported photocatalyst in the literatures.

Photocatalyst	**Amount of DBT (mg/L)**	**Light source**	**Removal efficiency (%)**	**Removal time (minute)**	**Ref.**
Au/TiO_2	200	UV	60	180	[27]
ZnO - Folded sheet mesoporous	250	UV	80	450	[28]
La/polyethylene glycol-modified TiO_2	250	UV	67.24	180	[29]
N-doped TiO_2	400	Visible	40.3	240	[30]
TiO_2 on the surface of FSM-16	400	UV	69	400	[32]
Ag@AgBr loaded mesoporous silica	500	Sunlight	98.66	360	[31]
PPy/g-C_3N_4	100	Sunlight	100	90	This work
	200			120	
	400			200	
	500			250	
	700			300	

3.5. Study real oilfield wastewater treatment

The photocatalytic applicity of the PPy/g-C_3N_4 nanocomposite was investigated for the treatment of 200 mL of 100 mg/L DBT solution collected from the wastewater treatment station of Daqing Oilfield, Songliao Plain in northeastern China, and compared to a control sample which was prepared from deionized water without any pollutants. Figure 7 shows the complete removal efficiency of DBT1 and DBT2 is obtained after 110 and 90 minutes of exposure to sunlight, respectively. It demonstrates that the existence of additional pollutants in oilfield wastewater can prolong comprehensive treatment of DBT1 derived from actual oilfield wastewater effluent. As a result, the findings show that PPy/g-C_3N_4 nanocomposite photodegrades efficiently for the removal of DBT molecules in actual oilfield wastewater.

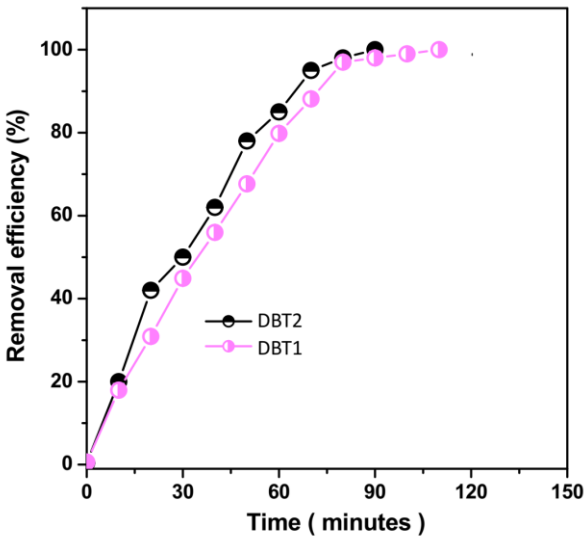

Figure 7. The comparison between the photocatalytic removal efficacies of 200 mL of 100 mg/L DBT solution provided from actual oilfield wastewater (DBT1) and control sample provided from deionized water (DBT2) using PPy/g-C_3N_4 nanocomposite upon sunlight irradiation.

4. CONCLUSION

This study concentrated on the chemical preparation of g-C_3N_4 and PPy/g-C_3N_4 nanocomposite, and characterization of structural, electrochemical and optical properties, as well as photocatalytic applicity for the removal of dibenzothiophene (DBT), an emerging organosulfur pollutant from oil field wastewater under exposure to sunlight. Analyses of photocatalyst structure and morphology revealed that PPy/g-C_3N_4 photocatalysts contained amorphous PPy nanoparticles that decorated the dense and thick layers of g-C_3N_4 which included the massive 2D sheet-like structure with numerous breakages and pores on the sheet surface that the g-C_3N_4 sheets created during melamine decomposition. Optical analyses revealed that the optical band gap values of g-C_3N_4 and PPy/g-C_3N_4 photocatalysts were determined to be ~2.64 and ~2.29 eV, respectively. This indicated a

decrease in the optical band gap of PPy/g-C_3N_4 toward g-C_3N_4, which enhanced the photocatalytic activity of PPy/g-C_3N_4 in the visible light region. Electrochemical studies revealed that the synergistic effect between PPy and g-C_3N_4 can effectively improve the electrochemical properties and increase the electron transfer rate. It was attributed to the smaller particle size of PPy decorated on the g-C_3N_4 sheet-like structure, which forms a large electroactive surface area and abundant electro-active sites in the PPy/g-C_3N_4 nanocomposite. Photocatalytic degradation studies revealed that total DBT treatment was obtained for g-C_3N_4 and PPy/g-C_3N_4 nanocomposite after 125 and 90 minutes of sunlight exposure, respectively. These findings demonstrated a faster photocatalytic treatment rate of DBT in the presence of PPy/g-C_3N_4 nanocomposite compared to other reported photocatalysts in the literature. This was due to the combination of PPy and g-C_3N_4 in the nanocomposite to create a large effective surface area and heterojunction to promote efficiency in photo-induced electrons and hole population and photocatalytic reactions. The practical photocatalytic degradation capability of PPy/g-C_3N_4 nanocomposite for the treatment of genuine oilfield wastewater was investigated, and the results demonstrated the effectual photocatalytic performance of PPy/g-C_3N_4 nanocomposite for the treatment of DBT in genuine oilfield wastewater.

References

1. L. Zhang, J. Huang, Z. Hu, X. Li, T. Ding, X. Hou, Z. Chen, Z. Ye and R. Luo, *Electrochimica Acta*, 422 (2022) 140553.
2. X. Tang, J. Wu, W. Wu, Z. Zhang, W. Zhang, Q. Zhang, W. Zhang, X. Chen and P. Li, *Analytical chemistry*, 92 (2020) 3563.
3. H. Karimi-Maleh, H. Beitollahi, P.S. Kumar, S. Tajik, P.M. Jahani, F. Karimi, C. Karaman, Y. Vasseghian, M. Baghayeri and J. Rouhi, *Food and Chemical Toxicology*, (2022) 112961.
4. J. Li, Z. Liang, Z. Chen, Z. Zhang, H. Liu, Z. Liu and Z. Xu, *Chemical Engineering Journal*, 453 (2022) 139767.
5. Z. Wu, C. Li, F. Zhang, S. Huang, F. Wang, X. Wang and H. Jiao, *Journal of Materials Chemistry C*, 10 (2022) 7443.
6. M. Yang, C. Li, Y. Zhang, D. Jia, X. Zhang, Y. Hou, R. Li and J. Wang, *International Journal of Machine Tools and Manufacture*, 122 (2017) 55.
7. F. Chen, J. Ma, Y. Zhu, X. Li, H. Yu and Y. Sun, *Journal of Hazardous Materials*, 426 (2022) 128064.
8. Z. Wan, T. Zhang, Y. Liu, P. Liu, J. Zhang, L. Fang and D. Sun, *Environmental Research*, 213 (2022) 113637.
9. M.-R. Wang, L. Deng, G.-C. Liu, L. Wen, J.-G. Wang, K.-B. Huang, H.-T. Tang and Y.-M. Pan, *Organic letters*, 21 (2019) 4929.
10. L. Zhang, Z. Hu, J. Huang, Z. Chen, X. Li, Z. Feng, H. Yang, S. Huang and R. Luo, *Journal of Advanced Ceramics*, 11 (2022) 1294.
11. W. Liu, J. Zheng, X. Ou, X. Liu, Y. Song, C. Tian, W. Rong, Z. Shi, Z. Dang and Z. Lin, *Environmental science & technology*, 52 (2018) 13336.
12. X. Cui, C. Li, Y. Zhang, Z. Said, S. Debnath, S. Sharma, H.M. Ali, M. Yang, T. Gao and R. Li, *Journal of Manufacturing Processes*, 80 (2022) 273.
13. R. Li, X. Qian, C. Gong, J. Zhang, Y. Liu, B. Xu, M.S. Humayun and Q. Zhou, *IEEE Transactions on Biomedical Engineering*, (2022) 1.
14. D. Jia, Y. Zhang, C. Li, M. Yang, T. Gao, Z. Said and S. Sharma, *Tribology International*, 169 (2022) 107461.

15. M. Yang, C. Li, Y. Zhang, Y. Wang, B. Li, D. Jia, Y. Hou and R. Li, *Applied Thermal Engineering*, 126 (2017) 525.
16. X. Zhang, C. Li, Y. Zhang, D. Jia, B. Li, Y. Wang, M. Yang, Y. Hou and X. Zhang, *The International Journal of Advanced Manufacturing Technology*, 86 (2016) 3427.
17. S. Zhao, H. Li, B. Wang, X. Yang, Y. Peng, H. Du, Y. Zhang, D. Han and Z. Li, *Fuel*, 321 (2022) 124124.
18. Z. Zhang, F. Yang, H. Zhang, T. Zhang, H. Wang, Y. Xu and Q. Ma, *Materials Characterization*, 171 (2021) 110732.
19. K.T. Silva, R.A. Oliveira-Castro, V.C. Rodrigues, W.G. de Lima, C.V. Rodrigues, W. Castro-Borges and M.H.r.G. Andrade, *Journal of Proteome Research*, 14 (2015) 385.
20. W. Liu, F. Huang, Y. Liao, J. Zhang, G. Ren, Z. Zhuang, J. Zhen, Z. Lin and C. Wang, *Angewandte Chemie*, 120 (2008) 5701.
21. X. Wang, C. Li, Y. Zhang, H.M. Ali, S. Sharma, R. Li, M. Yang, Z. Said and X. Liu, *Tribology International*, 174 (2022) 107766.
22. C. Yu, J.S. Qiu, Y.F. Sun, X.H. Li, G. Chen and Z.B. Zhao, *Journal of Porous Materials*, 15 (2008) 151.
23. A. Al-Abduly and V.K. Sharma, *Journal of hazardous materials*, 279 (2014) 296.
24. Y. Zhao and R. Wang, *Petroleum & Coal*, 55 (2013) 62.
25. S. Mishra, N. Pradhan, S. Panda and A. Akcil, *Fuel Processing Technology*, 152 (2016) 325.
26. G.O. Yahaya, F. Hamad, A. Bahamdan, V.V. Tammana and E.Z. Hamad, *Fuel processing technology*, 113 (2013) 123.
27. S. Khayyat and L.S. Roselin, *Journal of Saudi Chemical Society*, 21 (2017) 349.
28. A. Hosseini, H. Faghihian and A.M. Sanati, *Materials Science in Semiconductor Processing*, 87 (2018) 110.
29. S. Moradi, M. Vossoughi, M. Feilizadeh, S.M.E. Zakeri, M.M. Mohammadi, D. Rashtchian and A. Yoosefi Booshehri, *Research on Chemical Intermediates*, 41 (2015) 4151.
30. K. Kalantari, M. Kalbasi, M. Sohrabi and S.J. Royaee, *Ceramics International*, 42 (2016) 14834.
31. X.N. Pham, M.B. Nguyen, H.S. Ngo and H.V. Doan, *Journal of Industrial and Engineering Chemistry*, 90 (2020) 358.
32. A. Hosseini and H. Faghihian, *Journal of Industrial and Engineering Chemistry*, 76 (2019) 122.
33. H. Karimi-Maleh, C. Karaman, O. Karaman, F. Karimi, Y. Vasseghian, L. Fu, M. Baghayeri, J. Rouhi, P. Senthil Kumar and P.-L. Show, *Journal of Nanostructure in Chemistry*, 12 (2022) 429.
34. Y. Zhong, Z. Wang, J. Feng, S. Yan, H. Zhang, Z. Li and Z. Zou, *Applied surface science*, 295 (2014) 253.
35. H. Han, M. Fu, Y. Li, W. Guan, P. Lu and X. Hu, *Chinese Journal of Catalysis*, 39 (2018) 831.
36. T.-A. Shinozaki, M. Suenaga, Y. Ko, E. Yamamoto, H. Murayama and M. Tokunaga, *Journal of Cleaner Production*, 370 (2022) 133402.
37. H. Xing, L. Wu and X. Li, *International Journal of Electrochemical Science*, 17 (2022) 22066.
38. H. Salavati, A. Teimouri and S. Kazemi, *International Journal of Electrochemical Science*, 13 (2018) 2887.
39. N. Chi and W. Xu, *International Journal of Electrochemical Science*, 17 (2022) 220929.
40. M. Oves, M.O. Ansari, R. Darwesh, A. Hussian, M.F. Alajmi and H.A. Qari, *Coatings*, 10 (2020) 950.
41. Q. Wang, S. Wu, D. Cui, H. Zhou, D. Wu, S. Pan, F. Xu and Z. Wang, *Science of The Total Environment*, 850 (2022) 158034.
42. L. Tang, Y. Zhang, C. Li, Z. Zhou, X. Nie, Y. Chen, H. Cao, B. Liu, N. Zhang and Z. Said, *Chinese Journal of Mechanical Engineering*, 35 (2022) 1.
43. C. Zhang, J. Liu, X. Huang, D. Chen and S. Xu, *ACS Omega*, 4 (2019) 17148.
44. Y. Li, Q. Bai, Y. Guan, P. Zhang, R. Shen, L. Lu, H. Liu, X. Yuan, X. Miao and W. Han, *Nuclear Fusion*, 62 (2022) 076023.

45. T. Xiong, W. Cen, Y. Zhang and F. Dong, *Acs Catalysis*, 6 (2016) 2462.
46. Z. Tan, B. Dong, M. Xing, X. Sun, B. Xi, W. Dai, C. He, Y. Luo and Y. Huang, *Environmental Technology*, (2022) 1.
47. X. Wang, C. Li, Y. Zhang, Z. Said, S. Debnath, S. Sharma, M. Yang and T. Gao, *The International Journal of Advanced Manufacturing Technology*, 119 (2022) 631.
48. P. Sharma, P.P. Sarngan, A. Lakshmanan and D. Sarkar, *Journal of Materials Science: Materials in Electronics*, 33 (2022) 9116.
49. Y. Yang, Y. Gong, C. Li, X. Wen and J. Sun, *Journal of Materials Processing Technology*, 291 (2021) 117023.
50. W. Xu, C. LI, Y. Zhang, H.M. Ali, S. Sharma, R. Li, M. Yang, T. Gao, M. Liu and X. Wang, *International Journal of Extreme Manufacturing*, 4 (2022) 042003.
51. J. Rouhi, S. Mahmud, S.D. Hutagalung, N. Naderi, S. Kakooei and M.J. Abdullah, *Semiconductor Science and Technology*, 27 (2012) 065001.
52. Y. Liu, H. Zhang, Y. Lu, J. Wu and B. Xin, *Catalysis Communications*, 87 (2016) 41.
53. H.S. Abdulla and A.I. Abbo, *nternational Journal of Electrochemical Science* 7(2012) 10666.
54. R. Li, Z. Du, X. Qian, Y. Li, J.-C. Martinez-Camarillo, L. Jiang, M.S. Humayun, Z. Chen and Q. Zhou, *Quantitative Imaging in Medicine and Surgery*, 11 (2021) 918.
55. P. Liu, S. Li, L. Zhang, X. Yin and Y. Ma, *Catalysis Science & Technology*, 12 (2022) 4193.
56. J. Rouhi, S. Mahmud, S.D. Hutagalung and N. Naderi, *Electronics letters*, 48 (2012) 712.
57. X. Guo, K. Hu, M. Chu, Y. Li, J. Bian, Y. Qu, X. Chu, F. Yang, Q. Zhao and C. Qin, *ChemSusChem*, 13 (2020) 3707.
58. Z. Tan, H. Zhu, X. He, B. Xi, Y. Tian, X. Sun, H. Zhang and Q. Ouche, *Environmental Science and Pollution Research*, 29 (2022) 70269.
59. X. Dang, Z. Song and H. Zhao, *Sensors and Actuators B: Chemical*, 310 (2020) 127888.
60. Q. Song, S. Heng, W. Wang, H. Guo, H. Li and D. Dang, *Nanomaterials*, 12 (2022) 849.
61. J. Wang, Y. Xia, H. Zhao, G. Wang, L. Xiang, J. Xu and S. Komarneni, *Applied Catalysis B: Environmental*, 206 (2017) 406.
62. H. Li, Y. Zhang, C. Li, Z. Zhou, X. Nie, Y. Chen, H. Cao, B. Liu, N. Zhang and Z. Said, *The International Journal of Advanced Manufacturing Technology*, 120 (2022) 1.
63. Y. Zhang, C. Li, M. Yang, D. Jia, Y. Wang, B. Li, Y. Hou, N. Zhang and Q. Wu, *Journal of Cleaner Production*, 139 (2016) 685.
64. M.A. Mohamed, M. Zain, L.J. Minggu, M.B. Kassim, N.A.S. Amin, W. Salleh, M.N.I. Salehmin, M.F.M. Nasir and Z.A.M. Hir, *Applied Catalysis B: Environmental*, 236 (2018) 265.
65. B. Bai, F. Bai, X. Li, Q. Nie, X. Jia and H. Wu, *Environmental Technology & Innovation*, 28 (2022) 102944.
66. H. Karimi-Maleh, R. Darabi, M. Shabani-Nooshabadi, M. Baghayeri, F. Karimi, J. Rouhi, M. Alizadeh, O. Karaman, Y. Vasseghian and C. Karaman, *Food and Chemical Toxicology*, 162 (2022) 112907.
67. S.-X. Zhou, X.-Y. Tao, J. Ma, L.-T. Guo, Y.-B. Zhu, H.-L. Fan, Z.-S. Liu and X.-Y. Wei, *Vacuum*, 149 (2018) 175.
68. D. Ge, H. Yuan, J. Xiao and N. Zhu, *Science of The Total Environment*, 679 (2019) 298.
69. C. Liu and J. Rouhi, *RSC Advances*, 11 (2021) 9933.
70. H. Li, H. Tian, X. Wang, M. Pi, S. Wei, H. Zhu, D. Zhang and S. Chen, *ACS Applied Energy Materials*, 2 (2019) 4692.
71. Y. Wang, X. Wu, J. Liu, Z. Zhai, Z. Yang, J. Xia, S. Deng, X. Qu, H. Zhang and D. Wu, *Journal of Environmental Chemical Engineering*, 10 (2022) 107091.
72. C. Dong, Z. Wang, Z. Ye, J. He, Z. Zheng, X. Gong, J. Zhang and I.M. Lo, *Applied Catalysis B: Environmental*, 296 (2021) 120223.
73. Y. Nosaka and A. Nosaka, *ACS Energy Letters*, 1 (2016) 356.
74. L. Nan, C. Yalan, L. Jixiang, O. Dujuan, D. Wenhui, J. Rouhi and M. Mustapha, *RSC Advances*, 10

(2020) 27923.
75. B. Pare, S. Jonnalagadda, H. Tomar, P. Singh and V. Bhagwat, *Desalination*, 232 (2008) 80